

# **3D Mechanical Modeling of the Distribution of Fault Slip Rates in the Greater Los Angeles, CA Region**

**Hugh A. Harper**

**Department of Geology, Appalachian State University**

## **Abstract**

Geologic and geodetic studies have characterized slip rates for only a small portion of faults in the Los Angeles region, leaving many fault slip rates unconstrained. In this work, I use the Southern California Earthquake Center's Community Fault Model geometry and geodetic shortening rates combined with a mechanical model to calculate slip rates for 64 faults in the greater Los Angeles region. Model-predicted slip rates from the mechanical model, in most cases, fall within the range of geologic measurements. Furthermore, model-predictions and the geologic data do not systematically differ, suggesting that long- and short-term deformation rates are compatible. Because finite and nonplanar faults produce complex slip distributions, I also assess whether existing sites of geologic slip rate estimates are made at locations that the model predicts to be approximately average. I find that there is a slight tendency for sites of geologic slip rate estimates to be at locations where slip rates are faster than average for a given fault. Model results suggest that subsurface intersections of faults, which are typically geometrically unconstrained, greatly affect slip distribution for some faults. Some discrepancies between model predictions and geologic measurements suggest some unconstrained fault geometries in the CFM may inaccurate or that the tectonic shortening rates are significantly variable in some locations in the region.

## **Introduction**

The Los Angeles metropolitan region is situated south of the “Big Bend”, a major restraining bend in the right-lateral San Andreas Fault (Figure 1). This restraining bend places the Los Angeles region in a contractional tectonic regime with seismically active strike-slip (both

right- and left-lateral), reverse (high-angle and thrust), and oblique slip faults (Wright 1991). Global Positioning System measurements indicate that the region is currently shortening at a rate of  $4.5 \pm 1$  mm/yr (Argus, et al. 2005). The abundance of active faults in the region poses a significant hazard and risk to the greater Los Angeles region (Dolan, et al. 1995). To properly assess these hazards, knowledge of fault geometry and slip rates is essential (Field, et al. 2014, Field, et al. 2015).

### **Fault Slip Rates in the Los Angeles Region**

Geologic studies of faults in the region have characterized some of the major surface-breaching faults in the region using paleoseismic, tectonic geomorphology, and structural restoration methods (e.g., Morton and Matti 1987, Dolan, et al. 2000, Tsutsumi, et al. 2001, Crook, et al. 1987, Grant, et al. 1997, Stephenson, et al. 1995, Yeats, et al. 1994, Gath, et al. 1992). Structural modeling studies based on seismic reflection data have constrained several blind thrust fault slip rates in the subsurface (Oskin, et al. 2000, Huftile and Yeats 1996, Grant, et al. 1999, Shaw, et al. 2002). At the time of writing, a literature search has provided geologically-measured slip rates for 14 faults in the region, while the Southern California Earthquake Center (SCEC) Community Fault Model (CFM) suggests there are 64 active faults in the region. The lack of data on faults in the region leaves many fault slip rates unconstrained, and poses a challenge for seismic hazard analyses.

Existing deformation models in the Los Angeles region most often involve combining satellite geodetic data with kinematic modeling methods including block models (Meade and Hager 2005, Becker, et al. 2005) and various types of dislocation models (Savage and Burford

1973, Shen, et al. 1996, Zeng and Shen 2014). All deformation models require assumptions about fault geometries that must be carefully evaluated. For example, some models require faults to form a continuous network (i.e. block models) or to be infinite in length (i.e. two-dimensional models). These assumptions are often reasonable assumptions, especially in the case of very long faults such as San Andreas, or when modeling entire plate boundaries. However, current geological and geophysical data suggests that most faults in the greater Los Angeles region are short (10's of km) and discontinuous (e.g., Plesch, et al. 2007), so these plate-scale models, then, cannot accurately represent subsurface fault geometries shown in geologic and geophysical data or characterize slip distribution for shorter faults. The simplifications of plate-scale models lead to the exclusion of many of the faults in the region, and lead to significant shortcomings in assessing seismic hazard.

A fault which is finite in extent and not connected to other structures is predicted by fracture mechanics theory to have a distribution of slip across its surface with zero slip at the tip lines (e.g., Pollard and Segall 1987). This distribution of slip changes with interactions with nearby faults and fault topology (Bürgmann, et al. 1994, Marshall and Morris 2012). Mechanical interactions of finite non-planar faults are very complex and must be determined with the aid of a mechanical model (Marshall and Morris 2012, Marshall, et al. 2008) since mechanical interactions are not captured in kinematic models. The close spacing and complex geometries of the faults in Los Angeles region make it necessary to consider the effects of fault interactions on slip distributions when assigning a single slip rate (as is typically done in hazard assessments) to a fault.

To better constrain slip rates and slip distributions for the faults in the Los Angeles region, this study uses forward mechanical models driven by geodetically-constrained shortening rates. Fault geometries in the model are constrained by available geologic and geophysical data and come from the Southern California Earthquake Center (SCEC) Community Fault Model (CFM). Model results are then compared to existing geologic slip rate estimates to determine if the model is compatible with the longer term geologic data and to assess whether existing geologic estimates were made at locations that should yield approximately average slip behavior.

## **Three-Dimensional Mechanical Models of Faulting**

### **Fault Surface Geometry**

In this study, modeled fault surfaces use a tessellated triangular mesh based on the Southern California Earthquake Center (SCEC) Community Fault Model (CFM) version 5.0. The CFM representation of regional fault surfaces is constrained by all available geological and geophysical data, including seismic surveys, borehole data, earthquake hypocenters, and geologic mapping (Plesch, et al. 2007). An earlier version of this model (Marshall, et al. 2009) used fault surface geometries based on CFM version 2.5; however, many fault surfaces have undergone significant revisions in geometry in the latest revision of the CFM. For example, surface traces of nearly all faults in CFM 5.0 contain greater detail and new data from recent earthquakes has changed subsurface representations of some faults. As a result, the strike, dip, and surface area of many fault surfaces have been changed significantly. In addition to the updated fault geometries, the model has been expanded from 35 discrete fault surfaces and

5411 total elements (Marshall, et al. 2009) to include 64 discrete fault surfaces with 13,842 total elements throughout the greater Los Angeles region (Figure 2). This expansion is possible thanks to an increase in computing resources. Furthermore, the CFM 5.0 model presented here essentially combines the regions modeled in Marshall, et al. (2009) with those modeled in Marshall, et al. (2013), accounting for virtually all of the known active faults throughout the Transverse and Peninsular Ranges regions of southern California.

The raw CFM triangular mesh is spatially irregular, so it was necessary to remesh all of the fault surfaces to attain a more uniform element size and minimize numerical errors, yet still preserve the basic geometry of the fault surfaces. In the models presented here, the average element area is  $3.5 \text{ km}^2$  and the average element length is approximately 2.5 km. Element size varies throughout the model with generally smaller elements near the surface and increasing element size at depth. Thus, where the model is compared to the geologic data (i.e. the surface of the Earth), the model typically has the most geometric detail and best spatial resolution.

CFM surfaces extend only to seismogenic depths (15-19 km), but if a fault in a mechanical model were given a lower tipline, the slip would decrease with depth and the model would not be capable of producing long-term block-like offsets (Marshall, et al. 2009). Thus, in order to account for the deformation during the interseismic period, fault surfaces are projected down to greater depths. The Los Angeles Regional Seismic Experiment (LARSE) seismic data shows reverse faults in the region being truncated by a mid-crustal horizontal detachment (Fuis, et al. 2001). Past models of the Transverse Ranges have been shown to best fit geodetic data when reverse faults become horizontal at depth and strike-slip faults are semi-infinite in height (Shen, et al. 1996). Therefore, a basal horizontal crack in the model geometry

is employed for two reasons: first, it reproduces the reverse fault structure observed in seismic imagery while also allowing reverse faults to slip horizontally at depth. Second, it unpins the lower tip lines of strike-slip fault surfaces which simulates semi-infinite fault height. The depth at which the horizontal crack is placed does not affect strike-slip rates; however, dip slip rates will increase with the depth of the basal crack (Marshall, et al. 2009). The basal horizontal crack in this model is placed at 27.5 km depth, in agreement with LARSE data (Fuis, et al. 2001).

### **BEM Implementation of Geologic Timescale Deformation**

The Los Angeles regional fault network contains a complex network of interacting non-planar faults. While some faults in the region are well studied, the complete distribution of slip rates on any fault in the region is unknown. Given the relatively slow slip rates, close spacing, and small size of many of the regional faults, inverse geodetic methods are not likely to be reliable for estimating the distribution of slip rates on all faults in the CFM 5.0. Therefore, a forward model is used to calculate the mechanically- and kinematically-viable slip distributions throughout the fault network driven by far-field motions derived from GPS. To calculate the distribution of slip along interacting three-dimensional fault surfaces in response to regional shortening, I use a Boundary Element Method (BEM) implementation of long-term deformation (Marshall, et al. 2009, Marshall, et al. 2013) using the angular dislocation program, Poly3D (Thomas 1993), based on the BEM described in Comninou and Dundurs (1975). The mechanical modeling method and tectonic boundary conditions presented here closely follow those found in Marshall, et al. (2009) and Marshall, et al. (2013), but are briefly described here for clarity.

Rather than inverting geodetic data for slip rates or imposing slip rates on numerous dislocations, a regional shortening rate of 72 nanostrains/yr oriented at N9°E is implemented by applying displacements along the edges of a basal horizontal crack. This strain rate is consistent with geodetic strain rates measured in the region (Argus, et al. 2005, Marshall, et al. 2009). Once the region, as a whole, contracts at the regional geodetic strain rate, the CFM-based fault surfaces are inserted into the modeled half-space, allowing fault elements to freely slip and interact in response to the contraction. Fault elements are shear stress free and are not allowed to open or interpenetrate. Edge effects (related to the applied regional shortening) on the modeled faults are reduced by making the region of deformation (i.e. the basal crack) significantly larger than the area occupied by the modeled faults.

The effects of the San Andreas and San Jacinto faults were removed in the Argus, et al. (2005) GPS velocities so that only the strains due to Los Angeles faults remain. Since the model only concerns the Los Angeles region, the San Andreas and San Jacinto faults are also omitted from our models. Because of this omission, mechanical interactions with these faults are not present in this model, so slip behavior on faults near the northeastern edge of our model may be inaccurate.

A homogeneous and isotropic linear-elastic rheology are assumed throughout the model. Because of this rheologic assumption, some fault slip rates may mischaracterized if located near large sedimentary basins. Similar homogeneous isotropic rheologies are used in a wide range of models, including widely used block modeling techniques (e.g. Meade and Hager 2005, Becker, et al. 2005, Loveless and Meade 2011, McCaffrey 2005). Shear modulus of the medium is 30 GPa, and Poisson's ratio is 0.25. Model predictions are independent of shear

modulus. Variation in Poisson's ratio, when constrained to values found in the region's subsurface, does not significantly affect model predictions.

## Results

### **Model-Predicted Slip Rates and Comparisons to Geologic Data**

In addition to updated fault geometries and expanded region, I improve on past mechanical modeling efforts (Marshall, et al. 2009, Marshall, et al. 2013) by presenting more detailed comparisons with geologic data by comparing site-specific slip rates in the model to the geologic measurements for all of the faults for which data is available. I compare geologic timescale model predictions to geologic measurements of slip rates for three reasons: 1) to assess the accuracy of the mechanical model with respect to the geologic measurements, 2) to determine whether current regional geodetic shortening rates are compatible with longer term geologic measurements of fault slip rates, and 3) to test if existing geologic slip rate estimates were made in locations that should record approximately "average" slip rates. For modeled fault surfaces, the weighted average slip rate is calculated, which accounts for elements having differing surface areas. These average values are then compared to geologic measurements, either point measurements (paleoseismic or tectonic geomorphology studies) or structural analysis measurements. Since slip is spatially variable along faults (Bürgmann, et al. 1994), I also compare geologic point estimates to the model predicted value at a single element nearest to the geologic estimate. By comparing geologic estimates to model-predicted slip rates on the model elements most spatially proximal to the site of measurement, a more meaningful comparison can be made between the model predictions and the geologic estimates. If model-

predicted slip rates agree with the geologic measurements at the site of measurement, it is reasonable to expect that the model can be used to provide slip rate estimates for the numerous unconstrained faults in the region. Model predicted slip rates resulting from the CFM2.5 fault geometry (Marshall, et al. 2009) are compared to the CFM5.0 results and geologic measurements to determine if the newer CFM5.0 geometry results in a better fit to the geologic data. Figure 3 displays the comparisons made to the available geologic data, block model data, and previous CFM2.5 mechanical model predictions.

### **Reverse Slip Rate Comparisons**

First, I will consider the primarily reverse-slipping faults (Figure 3a). For the San Joaquin Hills, Santa Monica, and Sierra Madre East faults, all model predictions (CFM2.5 weighted average, CFM5.0 weighted average, and CFM5.0 site-specific) all fall within the geologic slip rate ranges. The geologic measurements on the Elysian Park fault place reverse slip rates in a range of 0.8 mm/yr to 2.2 mm/yr (Oskin, et al. 2000). Model predictions for reverse slip rates agree with the geology in CFM2.5 and slightly disagree with the geology in CFM5.0, where the model-predicted average slip rate is 0.4 mm/yr. Geologic measurements on the Northridge fault place reverse slip rates in a range of 0.35 mm/yr to 1.7 mm/yr (Huftile and Yeats 1996). Model predictions for reverse slip rates agree with geology in the CFM2.5 case, but the CFM5.0 model predicts an average reverse slip rate of 2.3 mm/yr. The Sierra Madre West fault is measured to reverse slip at a rate of 0.6 mm/yr to 2.2 mm/yr (Crook, et al. 1987, Rubin, et al. 1998). Model predictions for reverse slip rates agree with geology in the case of CFM2.5, the CFM5.0 model predicts an average reverse slip rate of 3.6 mm/yr and the site-specific prediction is even faster. The Cucamonga fault is measured to reverse slip at a rate of 4.5

mm/yr. Model results predict slower slip rates in CFM2.5 and significantly slower slip rates (difference of 3 mm/yr) in CFM5.0. The Cucamonga fault is on the edge of the modeled region, nearest to the San Andreas and San Jacinto Faults. Since these faults (and their interactions with nearby faults) are not captured in the model, a mismatch with geologic measurements is not surprising.

### **Strike Slip Rate Comparisons**

Now, I will consider the primarily strike-slip faults (Figure 3B). For the Chino, Hollywood, Newport-Inglewood, and Whittier faults, all model predictions (CFM2.5 weighted average, CFM5.0 weighted average, and CFM5.0 site-specific) match the geologic measurements. For the Raymond fault, only a minimum slip rate is available from geologic data at 1.5 mm/yr of left-lateral slip (Marin, et al. 2000). Model predicted left-lateral slip rates in all cases disagree with the geology and instead predict slower slip rates (1.1 mm/yr in CFM5.0, 0.4 mm/yr in CFM2.5). Geologic measurements for the San Gabriel fault give a range of right-lateral slip rates from 1.0 mm/yr to 2.5 mm/yr (Yeats, et al. 1994, Kahle 1986). Model-predicted right-lateral slip rates agree in the case of CFM5.0 (1.9 mm/yr) and slightly disagree in CFM2.5 (0.6 mm/yr). The Newport-Inglewood fault is measured to slip at a minimum 0.3 mm/yr right-laterally (Grant, et al. 1997). Since no geologic measurement for maximum slip rate is available, model predicted right-lateral slip rates for CFM2.5, CFM5.0, and site-specific slip are compatible with the geologic data. The Palos Verdes fault is measured to slip right-laterally with a rate ranging from 2.5 mm/yr to 3.8 mm/yr (Stephenson, et al. 1995). Model-predicted right-lateral slip rates agree in the case of CFM2.5 but disagree slightly in the case of CFM5.0 which predict an average slip rate of 4.4 mm/yr. A site-specific model prediction gives a right-lateral slip rate of 4

mm/yr, a slight improvement on the weighted average slip rate comparison. Reverse slip rate measurements are also available for the Palos Verdes fault (due to the reverse slip motion along a local restraining bend), with a lower limit of 0.26 mm/yr and an upper limit of 1.7 mm/yr (Huftile and Yeats 1996, Bryant 1987). Model-predicted average reverse slip rates agree in the case of CFM5.0 and slightly disagree in the CFM2.5 (0.1 mm/yr). The model-calculated site-specific slip rate corresponding to location of geologic slip measurement disagrees slightly with the geology with a slip rate of 1.9 mm/yr.

Comprehensive results for weighted-average slip rates on all of the modeled faults, including faults that have no other slip rate estimates, are provided in Table 1.

### **Model-Predicted Slip Rates and Comparisons to Existing Geodetic Models**

The model-predicted fault slip rates are also compared to block model slip rate estimates (Meade and Hager 2005) when available. Block model predictions fit the geologic measurements of slip rate for strike-slip faults well. The Meade and Hager (2005) block model does not attempt to model many reverse faults in the region, so most reverse faults in this study cannot be compared to the block model. There are three reverse faults included in the Meade and Hager (2005) model. Firstly, the Cucamonga fault, where predicted slip rates are compatible with the geologic data (since only a minimum slip rate is available for Cucamonga), whereas model predictions from this study were not. Secondly, the Sierra Madre East fault, where measured slip rates match the block model data (however, considering the large range of geologic measurements and block model predictions, this fit could be achieved with

significantly different rates). And lastly, the Sierra Madre West fault, where measured slip rates disagree with block models considerably.

Slip rate predictions from this study's model fit the geologic measurements as well or better than the predictions of block models with the exceptions of the Palos Verdes, Cucamonga, and Raymond faults. There is no evident trend of mismatch between block model predictions and this study's predictions, but block model predictions tend to predict faster slip rates than the mechanical model of this study (such is the case for six out of nine of the faults). While block models fit GPS data and characterize slip for major faults well, smaller faults and most reverse slip faults are left out of these simulations, leaving significant faults unassessed. The model presented here therefore has the advantage of including all of the known active faults in the region.

## **Discussion**

### **Reconciling Disagreement of Model Predictions with Geologic Measurements**

In the comparisons presented in the results sections, there are faults where neither weighted average slip rates nor site-specific slip rates agree with the geologic measurements. While the majority of the faults I compare do agree with geologic measurements, it is perhaps troublesome that there are cases of mismatch. Cases of mismatch must be reconciled with the geology in some way if model predictions are to be trusted. The cases of significant mismatch occur on the Cucamonga, Sierra Madre West, and Northridge faults.

Geologic data (Morton and Matti 1987) suggests that the Cucamonga fault is one of the fastest slipping faults in the region, yet the CFM5.0 model predicts a slip rate of about 1 mm/yr. This discrepancy partly arises as a result of the geometry contained in the CFM5.0 where the fault is modeled as a steeply-dipping fault which connects to no other fault in the vicinity. This geometry is constrained only by a surface trace with no subsurface data. Considering the very low model predictions for slip rate, a disconnected subsurface geometry and steep dip is likely not characteristic of the true fault geometry. In addition, the Cucamonga fault is located at the northeast edge of the modeled region, close to the San Andreas and San Jacinto faults. Since these faults are not included in the model, even if the fault geometry were accurately modeled, one would not expect it to match geologic measurements exactly because mechanical interactions with these fast-slipping and large faults are not accounted for in the model presented here.

If fault geometries are unconstrained at depth (such is the case with the Cucamonga fault) then it may be possible to reconcile discrepancies between the model and geology by manipulating the deep fault geometries. The Sierra Madre West fault is a case similar to Cucamonga, but the discrepancy is exactly the opposite: modeled fault slip rates are much too fast. This problem may be related to the Cucamonga fault issue. The two faults are part of a group of reverse-slipping faults. Despite this, the CFM5.0 geometry treats these as separate and disconnected faults in the subsurface. If, the Sierra Madre-Cucamonga fault system were connected in the subsurface, and the dip of Cucamonga were made more shallow, then it is likely that slip will be accommodated more evenly across the faults and model predictions may more closely match the geologic measurements.

The Northridge fault, a blind thrust which was the source of the 1994 M6.7 earthquake, is measured to reverse slip at a maximum of 1.7 mm/yr (Huftile and Yeats 1996) while the CFM5.0-based model predicts a weighted average slip rate of 2.3 mm/yr. Since the fault is not surface-breaching, there is no exact point location of slip rate measurement, so a site-specific comparison cannot be made. An important observation can be made about the Northridge fault: it is intersected by multiple faults in the subsurface, many more so in the CFM5.0 geometry than the CFM2.5 geometry. Interactions between faults near Northridge are complex and because these subsurface intersections are unconstrained, the fault interactions may not be accurately modeled in the CFM5.0.

### **Long Term Deformation and Short Term Deformation**

A potential issue with geodetic measurements of regional deformation is that currently observed deformation rates/patterns are potentially incompatible with geologic timescale deformation. If this were true, the geodetically-constrained model predictions presented here would be systematically different (too fast or too slow) in comparison to longer term geologic estimates of slip rates. Assuming model predictions are accurate, weighted average slip on faults can be compared to geologically-measured slip rates to assess whether geodetically-measured deformation rates (short term) are compatible with long term deformation rates. Figure 5 shows no systematic discrepancy between long term and short term slip rates; however, several faults suggest the short term rates (used in the model) are too fast in comparison to long term rates or that the 72 nstrain/yr shortening rate is variable throughout the modeled region.

## **Are Existing Geologic Slip Rates Average?**

Since the model, in most cases, appears to predict reasonable slip patterns (near the surface, most importantly), then its predictions can be used to determine if sites of existing geologic estimates are at locations where slip rate is characteristic or “average” for the fault as a whole. I compare the weighted average slip on faults to single element slip rates using an element closest to the location of measurement. Figure 6 shows the comparisons, with most faults plotting close to a 1:1 line. This suggests that existing site-specific geologic slip rate measurements in the region are typically reasonably characteristic of average fault slip behavior. Although only few in number, all of the outliers plot above the 1:1 line, suggesting surface-based site-specific measurements have a slight tendency to be faster than average fault slip. This observation is not completely unexpected: first, according to basic fault mechanics, surface-breaching faults should have fastest slip rates at the surface of the earth near the middle of the fault trace; second, geologic studies may be drawn to sites with relatively large geomorphic offsets where features are easier to measure accurately and slip rates might be faster than a fault’s average.

The Palos Verdes outlier is specifically the reverse slip measurement of the fault (the strike-slip site measurement is average). This discrepancy is expected because the site of measurement for reverse slip on the Palos Verdes fault (McNeilan, et al. 1996) is along a restraining bend in the fault where reverse slip rates would be expected to be anomalously high. Outside of the restraining bend, dip slip rates are nearly zero.

## **Fault Intersections and Interactions**

In a mechanical model, a single isolated fault will have a smoothly variable slip distribution along the fault surface; however, when a fault is intersected by another fault, large slip rate gradients and slip distribution discontinuities may occur. Because interactions and intersections in the subsurface partly control model-predicted slip distributions on many of the modeled faults, and because these intersections are almost always unconstrained, model-predicted slip patterns on single faults must be approached with some caution. When slip distribution on the modeled fault surfaces is visualized, many discontinuities in slip occur at subsurface intersections of faults. These intersections may result in highly variable slip patterns, even over relatively small distances. Therefore, in cases where a fault has several subsurface fault intersections, the slip distribution may deviate greatly from the typical pattern of maximum slip in the middle of a fault. Because of this, knowledge of subsurface fault intersections is key to correctly simulating the physics of a fault network as complex as the greater Los Angeles region.

An example where subsurface intersections and mechanical interactions control fault slip rate occurs on the Whittier fault (figure 4). At the surface alone, the Whittier fault is intersected by multiple other faults (Yorba Linda, Whittier Heights, Workman Hill, cf. Figure 1); however, in the subsurface, it is also intersected by the Puente Hills thrust (the Richfield and Coyote Hills segments), the Chino fault, and the Lower Elysian Park fault. Across the lines of intersection, there are several major gradients in slip rate (Figure 4), making the slip distribution discontinuous and quite variable over even small distances for the Whittier fault. The exact geometry of these and other subsurface fault intersections in the CFM are unconstrained by available data. If the physics of the complex Los Angeles fault network is to be

correctly simulated, these intersection geometries must be better constrained. Such subsurface intersections may also have significant implications for dynamic rupturing of the Los Angeles faults.

## Conclusions

With the exception of the Cucamonga, Sierra Madre West, and Northridge faults, the mechanical model-predicted slip rates for the faults in the Los Angeles region are compatible with existing geologic slip rate estimates. It therefore appears that geodetically-measured deformations rates of the Los Angeles region are generally compatible with longer term deformation rates measured by geologic studies on the majority of the faults in the region. Since no slip rate data is available for a large percentage of the faults in the region, predictions from the mechanical model in this study provide slip rate estimates that can be used in future seismic hazard assessments in the greater Los Angeles region (Table 1).

With the exceptions of Chino and Sierra Madre East, locations of geologic measurement in the region appear to have been made at sites where fault slip is approximately characteristic of a fault's average slip behavior. Reverse slip measurements on Palos Verdes appear to be non-average, but the measurement was made along a restraining bend in the right-lateral Palos Verdes fault, and is not expected to be average for the fault.

Future studies will involve a reworking of the Cucamonga-Sierra Madre fault geometry in hopes to reconcile the discrepancy between geologic measurements and model predictions. Since fault geometries are largely unconstrained at depth, this manipulation will not be in violation of any currently existing data. Further work may also include assessing CFM2.5

predictions versus CFM5.0 predictions and to determine which geometries are more representative of the actual fault geometries. Specifically, future studies should aim to better constrain the geometry of subsurface fault intersections. These subsurface fault intersections exert a strong control on the distributions of slip on some faults and are therefore key to properly simulating the physics of the Los Angeles fault system.

## Acknowledgements

I would like to thank the Appalachian State University Department of Geology and Office of Student Research, the NASA NC Space Grant, and the Southern California Earthquake Center for funding and partial support of this project.

## References

- Wright, T. L. (1991). Structural geology and tectonic evolution of the Los Angeles Basin, California, in *Active margin basins*, 35-134.
- Argus, D. F., M. B. Heflin, G. Peltzer, F. Crampé, and F. H. Webb (2005). Interseismic strain accumulation and anthropogenic motion in metropolitan Los Angeles, *Journal of Geophysical Research* **110**.
- Dolan, J. F., K. Sieh, T. K. Rockwell, R. Yeats, J. H. Shaw, J. Suppe, G. J. Huftile, and E. M. Gath (1995). Prospects for larger or more frequent earthquakes in the los angeles metropolitan region, *Science* **267** 199-205.
- Field, E. H., R. J. Arrowsmith, G. P. Biasi, P. Bird, T. E. Dawson, K. R. Felzer, D. D. Jackson, K. M. Johnson, T. H. Jordan, C. Madden, A. J. Michael, K. R. Milner, M. T. Page, T. Parsons, P. M. Powers, B. E. Shaw, W. R. Thatcher, R. J. Weldon, and Y. Zeng (2014). Uniform California Earthquake Rupture Forecast, Version 3 (UCERF3)—The Time-Independent Model, *Bulletin of the Seismological Society of America* **104** 1122-1180.
- Field, E. H., G. P. Biasi, P. Bird, T. E. Dawson, K. R. Felzer, D. D. Jackson, K. M. Johnson, T. H. Jordan, C. Madden, A. J. Michael, K. R. Milner, M. T. Page, T. Parsons, P. M. Powers, B. E. Shaw, W. R. Thatcher, R. J. Weldon, and Y. Zeng (2015). Long-Term Time-Dependent Probabilities for the Third Uniform California Earthquake Rupture Forecast (UCERF3), *Bulletin of the Seismological Society of America* **105** 511-543.
- Morton, D. M., and J. C. Matti (1987). The Cucamonga fault zone: Geologic setting and Quaternary history, in *Recent Reverse faulting the Transverse Ranges, California* D. M. Morton and R. F. Yerkes (Editors), United States Geological Survey, 179-203.
- Dolan, J. F., K. Sieh, and T. K. Rockwell (2000). Late Quaternary activity and seismic potential of the Santa Monica fault system, Los Angeles, California, *Geological Society of America Bulletin* **112** 1559-1581.

- Tsutsumi, H., R. S. Yeats, and G. J. Huftile (2001). Late Cenozoic tectonics of the northern Los Angeles fault system, California, Geological Society of America Bulletin **113** 454-468.
- Crook, R., Jr., C. R. Allen, B. Kamb, C. M. Payne, and R. J. Proctor (1987). Quaternary geology and seismic hazard of the Sierra Madre and associated faults, western San Gabriel Mountains, in *Recent Faulting in the Transverse Ranges, California* D. M. Morton and R. F. Yerkes (Editors), U. S. Geological Survey, 27-63.
- Grant, L. B., J. T. Waggoner, T. K. Rockwell, and C. von Stein (1997). Paleoseismicity of the north branch of the Newport-Inglewood fault zone in Huntington Beach, California, from cone penetrometer test data, Bulletin of the Seismological Society of America **87** 277-293.
- Stephenson, W. J., T. Rockwell, J. K. Odum, K. M. Shedlock, and D. A. Okaya (1995). Seismic Reflection and Geomorphic Characterization of the Onshore Palos Verdes Fault Zone, Los Angeles, California, Bulletin of the Seismological Society of America **85** 943-950.
- Yeats, R. S., G. J. Huftile, and L. T. Stitt (1994). Late Cenozoic tectonics of the East Ventura Basin, Transverse Ranges, California, AAPG Bulletin **78** 1040-1074.
- Gath, E. M., T. Gonzalez, and T. K. Rockwell (1992). Slip rate of the Whittier Fault based on 3-D trenching at Brea, Southern California, Abstracts with Programs - Geological Society of America **24**.
- Osokin, M., K. Sieh, T. K. Rockwell, G. Miller, P. Guptill, M. Curtis, S. McArdle, and P. Elliot (2000). Active parasitic folds on the Elysian Park anticline: Implications for seismic hazard in central Los Angeles, California, Geological Society of America Bulletin **112** 693-707.
- Huftile, G. J., and R. S. Yeats (1996). Deformation rates across the Placerita (Northridge M (sub w) = 6.7 aftershock zone) and Hopper Canyon segments of the western Transverse Ranges deformation belt, Bulletin of the Seismological Society of America **86** 3-18.
- Grant, L. B., K. J. Mueller, E. M. Gath, H. Cheng, R. Lawrence Edwards, R. Munro, and G. L. Kennedy (1999). Late Quaternary uplift and earthquake potential of the San Joaquin Hills, southern Los Angeles basin, California, Geology **27** 1031-1034.
- Shaw, J. H., A. Plesch, J. F. Dolan, T. L. Pratt, and P. Fiore (2002). Puente Hills blind-thrust system, Los Angeles California, Bulletin of the Seismological Society of America **92** 2946-2960.
- Meade, B. J., and B. H. Hager (2005). Block models of crustal motion in Southern California constrained by GPS measurements, Journal of Geophysical Research **110**.
- Becker, T. W., J. L. Hardebeck, and G. Anderson (2005). Constraints on fault slip rates of the southern California plate boundary from GSA velocity and stress inversions, Geophysical Journal International **160** 634-650.
- Savage, J. C., and R. O. Burford (1973). Geodetic determination of relative plate motion in central California, Journal of Geophysical Research **78** 832-845.
- Shen, Z. K., D. D. Jackson, and B. X. Ge (1996). Crustal deformation across and beyond the Los Angeles basin from geodetic measurements, Journal of Geophysical Research **101** 27,957-27,980.
- Zeng, Y., and Z.-K. Shen (2014). Fault network modeling of crustal deformation in California constrained using GPS and geologic observations, Tectonophysics **612-613** 1-17.
- Plesch, A., J. H. Shaw, C. Benson, W. A. Bryant, S. Carena, M. L. Cooke, J. F. Dolan, G. Fuis, E. Gath, L. Grant, E. Hauksson, J. H. Jordan, M. J. Kamerling, M. Legg, S. C. Lindvall, H. Magistrale, C. Nicholson, N. Niemi, M. Osokin, S. Perry, G. Planansky, T. K. Rockwell, P. Shearer, C. Sorlien, M. P. Süss, J. Suppe, J. Treiman, and R. Yeats (2007). Community Fault Model (CFM) for Southern California, Bulletin of the Seismological Society of America **97** 1793-1802.
- Pollard, D. D., and P. Segall (1987). Theoretical displacements and stresses near fractures in rock: with applications to faults, joints, veins, dikes, and solution surfaces, in *Fracture Mechanics of Rock*, Academic Press Inc., London, 277-349.
- Bürgmann, R., D. D. Pollard, and S. J. Martel (1994). Slip distributions on faults: effects of stress gradients, inelastic deformation, heterogeneous host-rock stiffness, and fault interaction, Journal of Structural Geology **16** 1675-1690.

- Marshall, S. T., and A. C. Morris (2012). Mechanics, slip behavior, and seismic potential of corrugated dip-slip faults, *Journal of Geophysical Research* **117**.
- Marshall, S. T., M. L. Cooke, and S. E. Owen (2008). Effects of non-planar fault topology and mechanical interaction on fault slip distributions in the Ventura Basin, California, *Bulletin of the Seismological Society of America* **98** 1113-1127.
- Marshall, S. T., M. L. Cooke, and S. E. Owen (2009). Interseismic deformation associated with three-dimensional faults in the greater Los Angeles region, California, *Journal of Geophysical Research* **114** 1-17.
- Marshall, S. T., G. J. Funning, and S. E. Owen (2013). Fault slip rates and interseismic deformation in the western Transverse Ranges, CA, *Journal of Geophysical Research* **118** 4511-4534.
- Fuis, G. S., T. Ryberg, N. J. Godfrey, D. A. Okaya, and J. M. Murphy (2001). Crustal structure and tectonics from the Los Angeles basin to the Mojave Desert, southern California, *Geology* **29** 15-18.
- Thomas, A. L. (1993). POLY3D: A three-dimensional, polygonal element, displacement discontinuity boundary element computer program with applications to fractures, faults, and cavities in the Earth's crust, Stanford University, 52.
- Comninou, M. A., and J. Dunders (1975). The angular dislocation in a half-space, *Journal of Elasticity* **5** 203-216.
- Loveless, J. P., and B. J. Meade (2011). Stress modulation on the San Andreas fault by interseismic fault system interactions, *Geology* **39** 1035-1038.
- McCaffrey, R. (2005). Block kinematics of the Pacific-North America plate boundary in the southwestern United States from inversion of GPS, seismological, and geologic data, *Journal of Geophysical Research* **110**.
- Rubin, C. M., S. C. Lindvall, and T. K. Rockwell (1998). Evidence for large earthquakes in metropolitan Los Angeles, *Science* **281** 398-402.
- Marin, M., J. F. Dolan, R. D. Hartleb, S. A. Christofferson, A. Z. Tucker, and L. A. Owen (2000). A latest Pleistocene-Holocene slip rate on the Raymond fault based on 3-D trenching, East Pasadena, California, *Eos Trans. AGU* **81**.
- Kahle, J. E. (1986). The San Gabriel fault near Castaic and Saugus, Los Angeles County, California Division of Mines and Geology 8.
- Bryant, M. E. (1987). Emergent marine terraces and Quaternary tectonics, Palos Verdes Peninsula, California, in *SEPM Guidebook*, 63-78.
- McNeilan, T. W., T. Rockwell, and G. S. Resnik (1996). Style and rate of Holocene slip, Palos Verdes Fault, Southern California, *Journal of Geophysical Research* **101** 8317-8334.

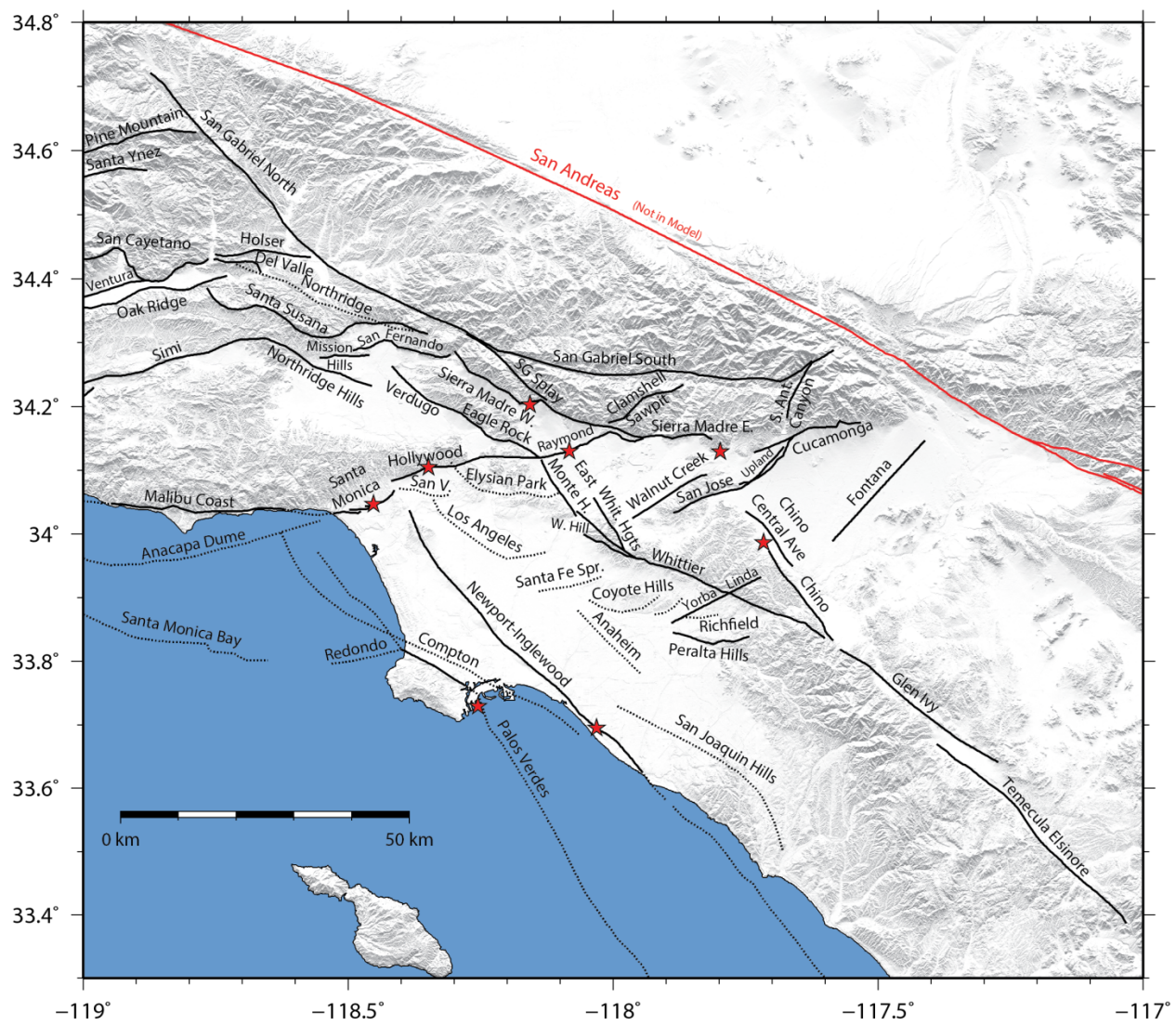


**Figure 1.** The Los Angeles metropolitan region and associated faults. Surface traces of surface-breaching faults are shown with solid lines; upper tip lines of blind faults and offshore faults are shown with dotted lines. The San Andreas Fault to the north (red line) is not included in the models presented here but is shown for location purposes. Locations of geologic slip estimates from the literature are shown with red stars.

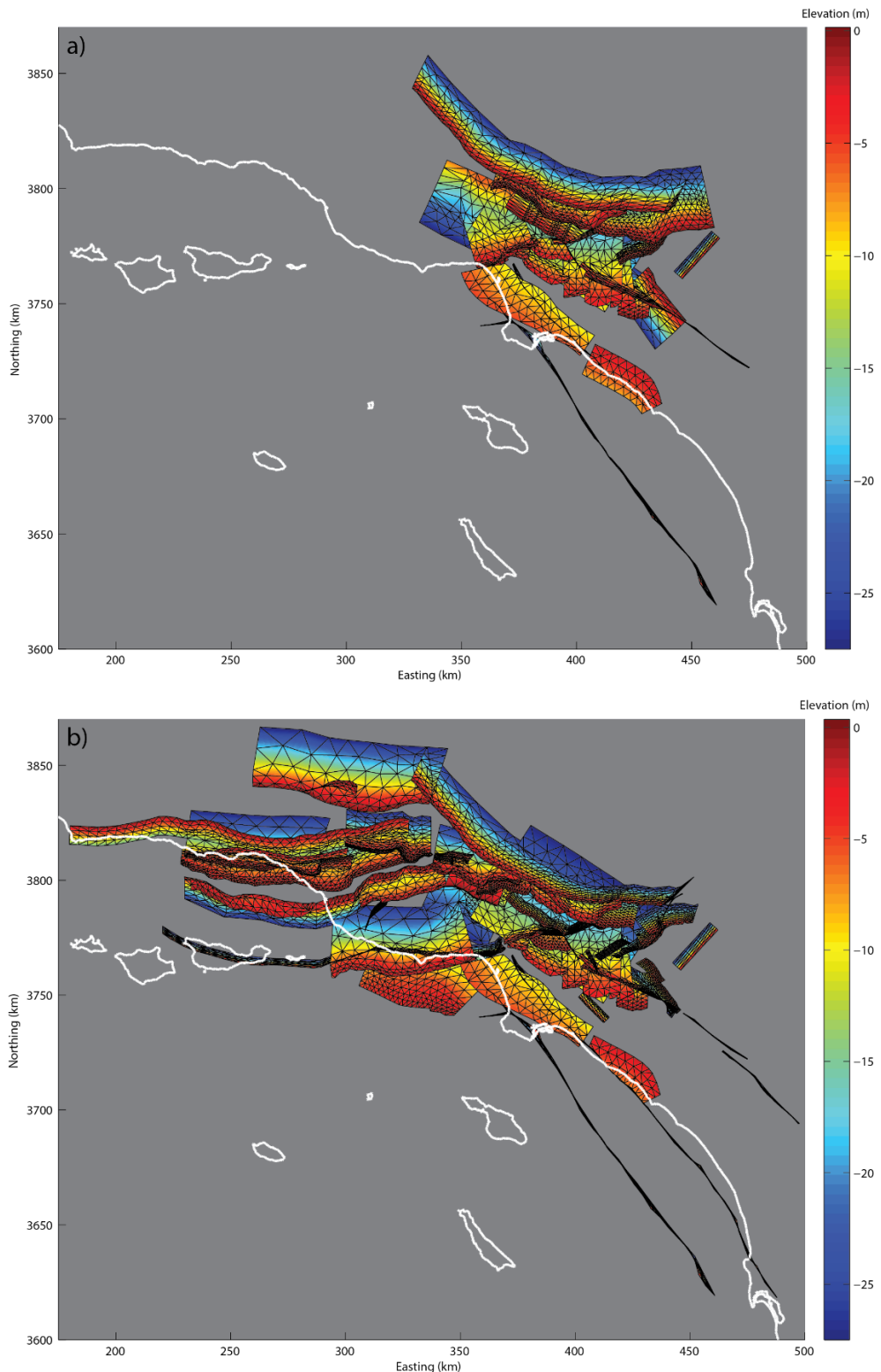


**Figure 2.** A) Modeled fault geometry for Community Fault Model (CFM) version 2.5 (Marshall et al., 2009). The thick white line indicates the coast line. Projection is UTM. This model includes 35 faults and a total of 5411 elements. B) Modeled fault geometry for Community Fault Model (CFM) version 5.0. This model includes 64 faults and a total of 13842 elements.

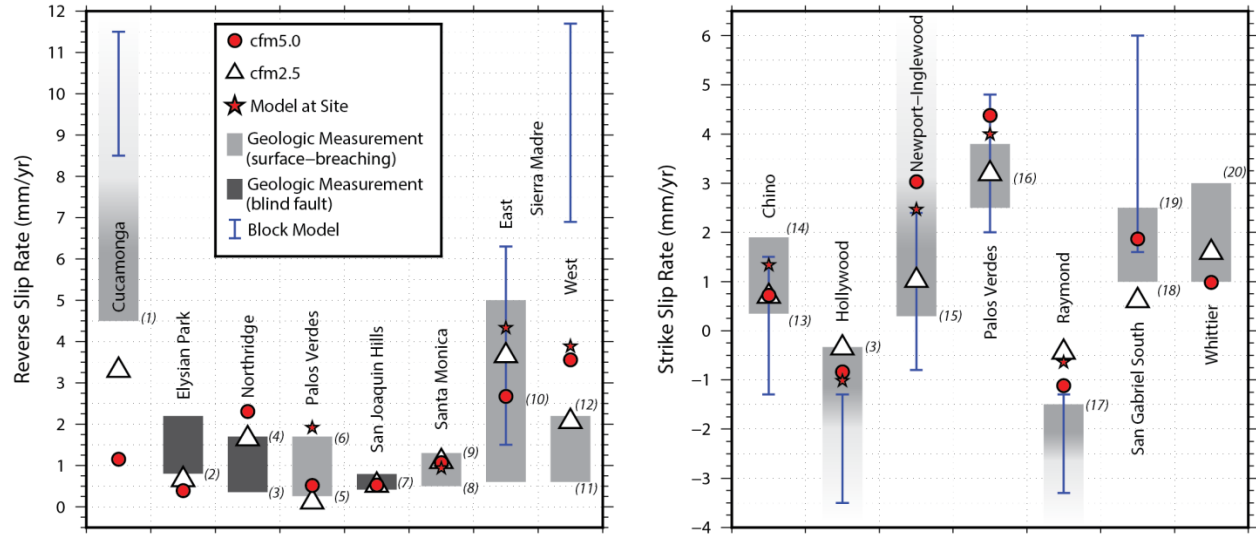


**Figure 3.** Comparisons of model-predicted slip rates (both weighted-average and site-specific, if applicable) for all faults where geologic data are available. Bars with gradients indicate a fault with only a minimum geologic slip rate estimate. Geologic slip rate estimates labeled on the plot are as follows: 1) Morton and Matti (1987), 2) Oskin, et al. (2000), 3) Dolan, et al. (1997), 4) Huftile and Yeats (1996), 5) Bryant (1987), 6) McNeilan, et al. (1996), 7) Grant, et al. (1999), 8) Dolan, et al. (2000), 9) Tsutsumi, et al. (2001), 10) Tucker and Dolan (2001), (11) Rubin, et al. (1998), 12) Crook, et al. (1987), 13) Walls and Gath (2001), 14) Yeats (2002), 15) Grant, et al. (1997), 16) Stephenson, et al. (1995), 17) Marin, et al. (2000), 18) Kahle (1986), 19) Yeats, et al. (1994), 20) Gath, et al. (1992).

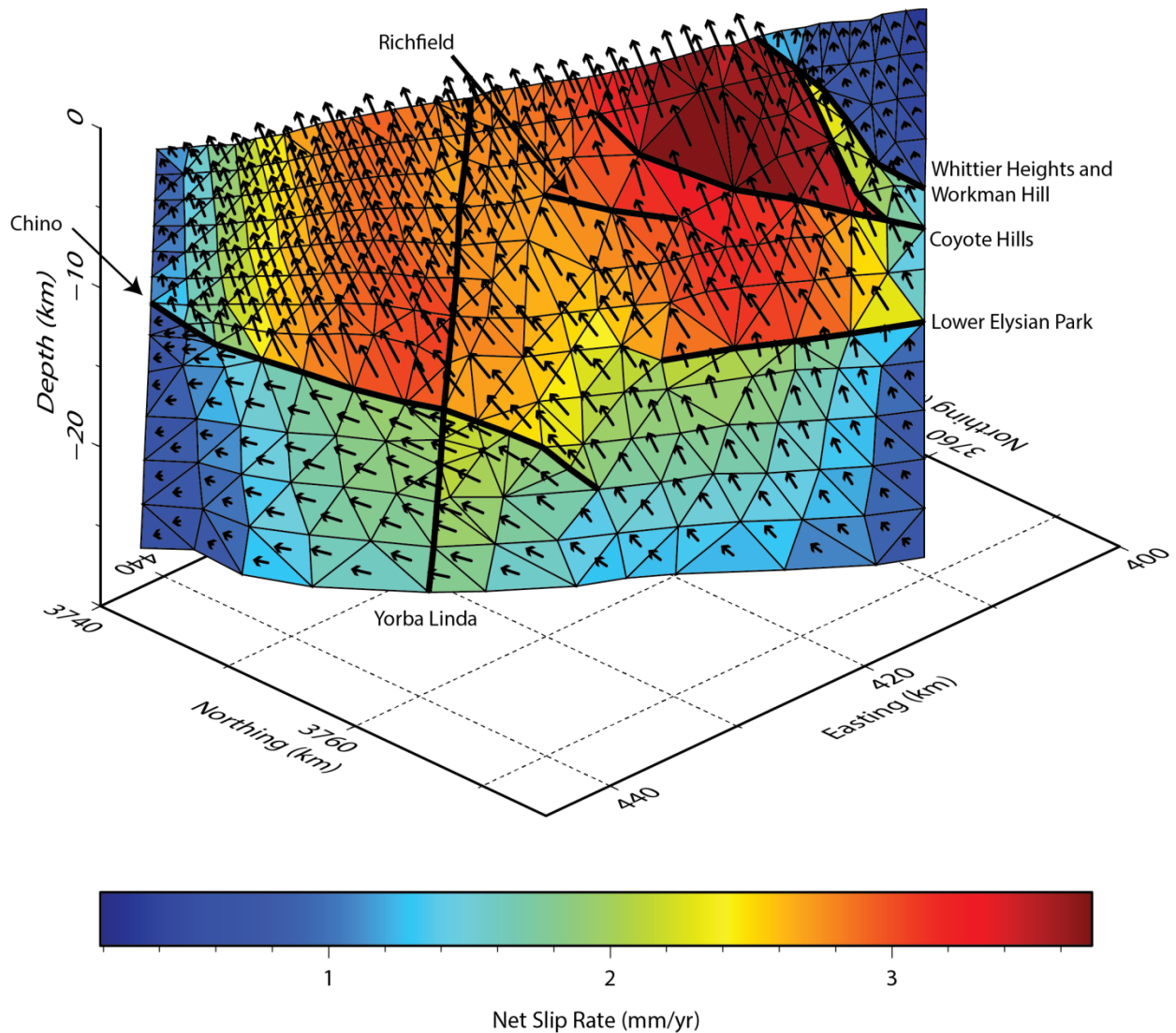


**Figure 4.** Slip distribution map of the Whittier fault from CFM 5.0. Projection is UTM, and the view is oblique. Major fault intersections are shown with thick black lines. Notice that discontinuities in slip rate occur at most of these intersections. The Richfield intersection is an exception due to its relatively slow slip rate. Because nearly all subsurface fault intersections are unconstrained, the model-predicted patterns could significantly change with updates to the CFM.

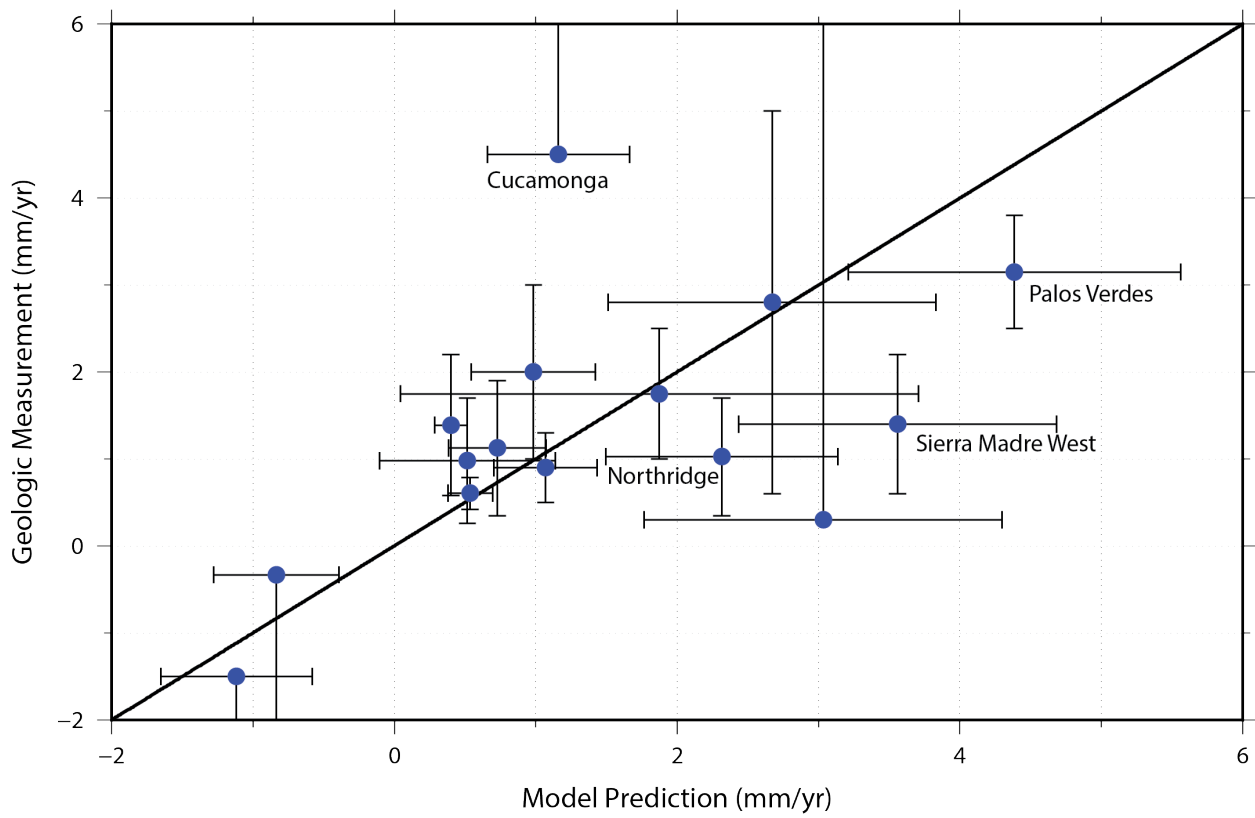


**Figure 5.** A comparison of short-term deformation rates (weighted average model predictions) to long-term deformation rates (geologic measurements). Error bars for model predictions are one standard deviation of weighted average slip for faults. One-sided vertical error bars are for faults that only have minimum geologic slip rate estimates. Outliers are present (labeled with text), but no systematic differences are evident.

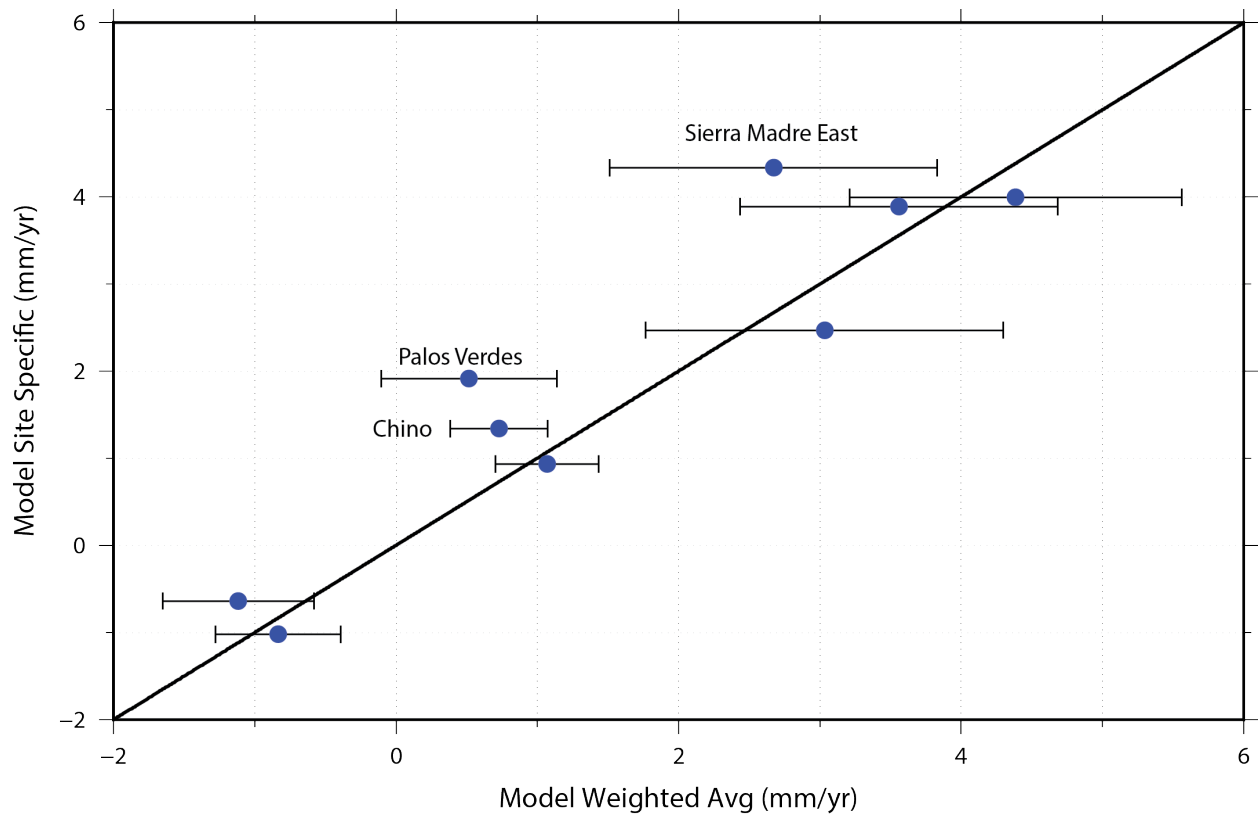


**Figure 6.** Comparison of model calculated fault average slip to single element slip at location of geologic measurements. Error bars show the standard deviation of weighted average slip on faults for model predictions. Locations of past geologic slip rate measurements appear to be about average for faults in the region, with a slight tendency to overestimate slip rate compared to the model-predicted fault average.

**Table 1.** Model-predicted weighted average slip rates (in mm/yr) for Los Angeles regional faults

Fault	Dip Slip	$\sigma$	Strike Slip	$\sigma$	Net Slip	$\sigma$
Anacapa Dume	3.17	1.33	-0.48	0.79	3.21	1.55
Anaheim	0.24	0.06	0.12	0.07	0.27	0.10
Bailey	0.12	0.12	-0.32	0.20	0.34	0.23
Big Pine	0.03	0.18	-0.21	0.17	0.21	0.24
Channel Islands Thrust	1.06	0.44	-0.04	0.27	1.06	0.52
Chino	1.39	0.75	0.73	0.34	1.57	0.83
Clamshell-Sawpit Canyon	0.78	0.22	-0.58	0.16	0.97	0.27
Compton	0.57	0.25	0.33	0.67	0.66	0.72
Coronado	0.17	0.15	4.59	1.20	4.59	1.21
Coyote Hills	0.89	0.47	-0.31	0.29	0.94	0.55
Cucamonga	1.16	0.50	-0.61	0.31	1.31	0.59
Del Valle	0.03	0.11	0.00	0.13	0.03	0.17
East Montebello	0.48	0.20	0.44	0.13	0.65	0.23
Elysian Park	0.40	0.12	0.01	0.10	0.40	0.15
Fontana	0.37	0.13	-1.20	0.27	1.25	0.30
Glen Ivy	0.01	0.12	1.67	0.50	1.67	0.52
Hollywood	1.12	0.32	-0.84	0.44	1.40	0.55
Holser	0.85	0.36	-0.36	0.19	0.93	0.41
Lion	0.17	0.15	-0.39	0.25	0.42	0.29
Los Angeles-Steep	1.21	0.36	0.04	0.22	1.21	0.42
Lower EP	3.22	1.72	1.20	1.06	3.44	2.02
Malibu Coast	1.32	0.64	-0.78	0.54	1.53	0.84
Mid-Channel	0.26	0.15	0.22	0.20	0.34	0.25
Mission Hills	0.29	0.08	-0.28	0.07	0.40	0.11
Mission Ridge-Arroyo Parida	0.80	0.36	-0.25	0.38	0.84	0.52
Newport-Inglewood	0.10	0.14	3.03	1.27	3.04	1.27
Northridge	2.31	0.82	0.82	0.73	2.46	1.10
Northridge Hills	1.00	0.39	-0.03	0.18	1.00	0.43
North Salt Lake	0.12	0.06	-0.16	0.06	0.20	0.09
Oak Ridge Offshore	1.12	0.38	0.14	0.59	1.12	0.70
Oak Ridge Onshore	1.46	0.40	-1.19	0.46	1.88	0.61
Palos Verdes	0.52	0.62	4.39	1.18	4.42	1.33
Peralta Hills	0.75	0.24	-0.18	0.15	0.77	0.28
Pine Mountain	6.30	1.48	1.01	0.62	6.38	1.61
Raymond	1.16	0.45	-1.12	0.53	1.61	0.70
Red Mountain	4.12	1.17	0.19	0.58	4.12	1.30
Redondo Canyon	0.29	0.20	-0.01	0.16	0.29	0.26
Richfield	0.47	0.19	-0.26	0.26	0.54	0.33
Rose Canyon	0.11	0.12	3.64	0.88	3.65	0.89
San Antonio Canyon	0.12	0.11	-0.35	0.10	0.37	0.15
San Cayetano	1.55	0.39	-0.26	0.38	1.57	0.54
San Fernando	1.64	0.73	-0.14	0.37	1.65	0.82
San Gabriel North	2.73	1.95	5.26	1.70	5.93	2.58
San Gabriel South	1.70	1.69	1.87	1.83	2.53	2.49
San Gabriel Splay	0.39	0.30	0.83	0.41	0.92	0.51
San Joaquin Hills	0.54	0.16	0.25	0.10	0.59	0.19
San Jose	1.05	0.40	-1.31	0.44	1.68	0.60
Santa Cruz Island	1.15	0.59	0.89	0.63	1.45	0.86
Santa Fe Springs	1.10	0.41	-0.21	0.21	1.12	0.46
Santa Monica	1.07	0.37	-1.17	0.37	1.59	0.52
Santa Monica Bay	1.11	0.42	0.17	0.26	1.12	0.50
Santa Rosa Island	0.89	0.30	-0.13	0.39	0.90	0.49
Santa Susana	2.14	0.73	-0.89	0.83	2.32	1.11
Santa Ynez	1.44	0.82	-0.52	0.40	1.53	0.91
Santa Ynez Valley	0.16	0.11	0.52	0.15	0.54	0.18
San Vicente	0.59	0.22	-0.16	0.09	0.61	0.23
Sierra Madre East	2.67	1.16	0.08	0.63	2.67	1.32
Sierra Madre West	3.56	1.13	0.78	0.50	3.64	1.23
Simi	1.01	0.41	-0.87	0.30	1.33	0.51
Temecula Elsinore	0.12	0.12	2.11	0.54	2.11	0.56
Uplands	0.52	0.26	-0.55	0.52	0.76	0.58
Ventura	2.28	1.17	-0.89	0.99	2.45	1.54
Verdugo-EagleRock	1.49	0.32	0.65	0.24	1.62	0.40
Walnut Creek	0.36	0.14	-0.41	0.16	0.55	0.21
Whittier	1.74	1.04	0.98	0.44	2.00	1.13
Whittier Heights	0.60	0.16	0.76	0.22	0.97	0.27
Workman Hill	1.23	0.25	0.45	0.20	1.31	0.32
Yorba Linda	0.27	0.22	-0.82	0.33	0.86	0.40